BABEȘ-BOLYAI UNIVERSITY

FACULTY OF PHYSICS

DOCTORAL SCHOOL OF PHYSICS

TiO_2 photocatalysts: environmental impacts and alternatives

Ph.D. Thesis

Scientific advisor:

Prof. dr. habil. Lucian Baia

Ph.D. Student:

Kata Saszet

Cluj-Napoca

2025

Table of contents

1. Introduction

Through collaborative efforts, science and industry have developed a variety of novel water remediation processes to address pollution caused by contaminants of emerging concern (CECs), which conventional treatment methods cannot efficiently remove. One important category of these techniques is the advanced oxidation processes (AOPs) [1]. Among these, heterogeneous photocatalysis has gained great appeal in recent decades due to its high removal efficiency of a broad range of organic pollutants. One of the most promising aspects of heterogeneous photocatalysis is its potential environmental sustainability. With the use of a suitable photocatalyst, this method can harness solar energy to fully mineralize organic contaminants into benign end products such as water and carbon dioxide [2]. Additionally, due to the two different phases present in the photocatalytic system – the solid photocatalyst and the pollutant in the aqueous media – the retention of the spent photocatalyst at the end of the process is relatively facile.

Titanium dioxide (TiO_2) was the first semiconductor employed in photocatalytic processes, introduced by Fujishima and Honda in 1972 for photocatalytic water splitting [3]. Since then, it has remained the most widely applied photocatalyst, primarily due to its excellent performance under UV light. However, significant research over the past decades has focused on extending TiO_2's photocatalytic activity to the solar spectrum, improving its efficiency, and making the process more feasible for large-scale applications. The process of researching and developing novel, high-performant nanomaterials for photocatalysis involves numerous synthesis approaches, several harsh chemicals, costly and complex processes, and the generation of various by-products [4]. Examining the overall process of heterogeneous

photocatalysis reveals that these aspects of photocatalyst production challenge its classification as an environmentally friendly solution.

With the growing industrial production of nano TiO_2 and its uncontrolled environmental release, accumulation has been observed in both our technical and natural environment. Moreover, the increasing accumulation values suggested by the predictive models raise growing concerns of ecotoxicity [5]. The toxicity of TiO_2 through various routes of exposure and on several model organisms has been investigated comprehensively, but the main focus of these studies was on the directly observable outcomes of TiO_2 exposure. One of the main proposed mechanisms of TiO_2 toxicity is the oxidative stress caused by the reactive oxygen species (ROS) generated by the semiconductor [6].

Literature on the indirect and long-term ecological effects of environmental release of TiO_2, particularly on the behavior and community structure of species, is scarce. Social insects, such as ants, are particularly vulnerable to the effects of the photocatalytic properties of TiO_2, due to their reliance on chemical cues. Nevertheless, the possibility of photocatalytic oxidation of these endobiotic molecules had not been previously considered.

For the reduction of environmental release and prevention of nano TiO_2 impact on the natural environment, one proposed solution is the magnetic separation of photocatalysts post-treatment, allowing for their recovery and reuse. This process involves the introduction of TiO_2 in composites with magnetic nanoparticles, such as Fe_3O_4 (magnetite). The main challenge of this method lies in the stabilization of iron oxide within the composite matrix, which is critical for ensuring consistent photocatalytic performance and maintaining recyclability [7,8].

The optimization of the TiO_2 photocatalyst, besides improving its efficiency, must also involve the development of a simple and feasible preparation method using potentially environmentally friendly materials and fewer by-products. The naturally occurring mineral form of TiO_2, rutile, is primarily used as a raw material in industrial production. Although previously overlooked in heterogeneous photocatalysis due to its impurity content and limited tunability, recent studies suggest that, with appropriate processing, natural rutile may serve as a promising alternative source of TiO_2 photocatalysts [9].

2. The main objectives of the Ph.D. thesis

The main aim of the thesis is the investigation of the potential environmental impact of the synthetic TiO_2 photocatalyst and the study of two alternative methods for the potential mitigation of this impact. The main objective is achieved by an interdisciplinary research that branches into three directions: assessment of the ecotoxicological effects of commercial TiO_2 on ant communication; investigation of the separability and recyclability of magnetically separable TiO_2 composites to reduce environmental release; and investigation of the photocatalytic potential of natural rutile TiO_2 minerals as alternative photocatalyst sources.

3. Outline and structure of the Ph.D. thesis

The Ph.D. thesis consists of five chapters followed by a reference section, acknowledgments, annexes of the scientific work, and a presentation of the Ph.D. candidate's scientific activity.

Chapter 1 outlines the motivation behind the scientific work of the thesis, presents the theoretical aspects related to TiO_2 photocatalysts and the key observations of previous literature, and defines the objectives of the thesis. Chapters 2, 3, and 4 highlight three interconnected scientific research topics that investigate the environmental impact of TiO_2 photocatalysts and alternative solutions. The following section outlines the steps taken to achieve the main objectives, presented in the structure of Chapters 2, 3, and 4.

Chapter 2. Investigation of ecotoxicity and photocatalytic removal of a trail pheromone by Evonik AEROXIDE P25 TiO_2.

- Investigation of the ecotoxicity of TiO_2 with respect to the foraging behavior of the ant *Lasius niger*.
- Evaluation of the photocatalytic degradation of a pheromone-related organic compound by TiO_2.

Chapter 3. Investigations of Fe_3O_4 loaded TiO_2 photocatalytic systems.

- Preparation of magnetically separable Fe_3O_4 loaded TiO_2 composites.
- Assessment of the photocatalytic efficiency of magnetic TiO_2 composites for paracetamol removal under UV light.
- Evaluation of the separability and reusability of magnetic composites.
- Investigation of correlations of structural, optical, and surface properties, photocatalytic efficiency, and reusability.

Chapter 4. Visible light active natural rutile photocatalyst obtained *via* nano milling.

- Exploration of a processing method of rutile minerals for use in visible-light-driven photocatalysis.
- Investigation of the structural, optical, and surface properties of the processed minerals.
- Assessment of the photocatalytic performance of natural rutile in removing phenol and ibuprofen under visible light irradiation.
- Establishing correlations between structural, optical, and surface properties of rutile and its photocatalytic activity.
- Analysis of the cost-benefit trade-off between natural rutile mineral and commercial Evonik Aeroxide P25 TiO_2 in heterogeneous photocatalysis applications.

The thesis ends with **Chapter 5, Final remarks and conclusions**, highlighting the key findings of the presented research.

4. Methods and Instrumentation

4.1. Pheromone-based foraging test method in the presence of TiO_2

To assess the impact of TiO_2 nanoparticles on pheromone-based foraging behavior in ants, a laboratory ecotoxicological test was conducted using the model species *Lasius niger* (black garden ant). Ant foragers were collected from a natural colony and acclimated in four artificial nests for two weeks under controlled conditions. Before testing, feeding was discontinued for three days to encourage foraging activity. The experimental setup included a water-filled plastic box connected to a nest by a plastic tube, with a diamond-shaped paper bridge suspended above the water, leading to a food source

(***Figure 1a.***). The bridge had two identical branches: one treated with an aqueous TiO_2 suspension (1 $g \cdot L^{-1}$) and the other with distilled water. Negative controls had both branches treated with water; positive controls had both treated with TiO_2 suspension (***Figure 1b.***).

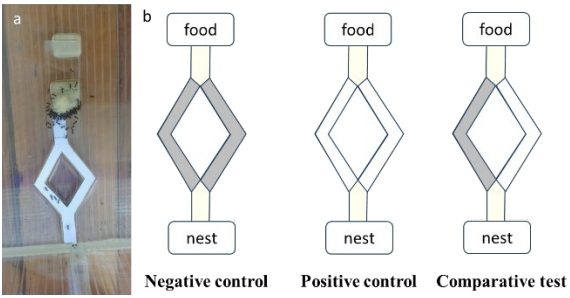

Figure 1.*a. Experimental setup. b. Sketch of the experimental set-up and the test types (grey - distilled water treatment; white - TiO_2 suspension treatment).*

Each experiment was performed under UV-A light (6 W, λ_{max} = 365 nm) to activate TiO_2's photocatalytic properties. New bridges and food were used for every trial. Comparative tests were conducted in 12 replicates, controls in 5, with random nest assignment to eliminate memory bias. Ant crossings at the bridge center were counted every minute for 9 minutes, starting with the first crossing. The statistical analyses were carried out in the R software environment (lme4 package) to analyze generalized linear mixed models (GLMM, Poisson distribution), with branch treatment as the input variable and ant crossings as the output. The individual test identifier was used as a random effect to account for variation across replicates.

4.2. Preparation of magnetically separable Fe_3O_4 loaded TiO_2 composites

Iron oxide nanoparticles (IONPs) were synthesized by a controlled precipitation method, using $FeCl_2 \cdot 4H_2O$ (0.2 M) precursor. Four samples were gained by the variation of experimental conditions, namely the alkalinity of the solution and temperature (***Figure 2***). The sample IONP_0.8_75 was chosen to be introduced in a composite with TiO_2 due to its favorable primary crystallite size and predominantly magnetite crystal phase.

	0.4 M NaOH	**0.8 M NaOH**
25 °C	33.3 nm	23.2 nm
75 °C	43.7 nm	46.4 nm

Figure 2. *Synthesis conditions and resulting primary crystallite size in the case of IONP samples.*

For the photocatalyst part of the composites, two TiO_2 samples were chosen. The first TiO_2 was synthesized *via* the hydrothermal crystallization method from titanium (IV) isopropoxide (TTIP), yielding a pure anatase crystal phase with 9.2 nm primary crystallite size (named TH). The second was a reference, the commercial Evonik Aeroxide P25, with mean crystallite sizes of 24 nm (anatase) and 36 nm (rutile), named P25.

To prepare the TiO_2-Fe_3O_4 composites, either commercial P25 TiO_2 or anatase TiO_2 was added to the synthesis solution of the iron oxide nanoparticle IONP_0.8_75. The $FeCl_2 \cdot 4H_2O$ concentration was reduced to 0.05 M, and the mixture was prepared to achieve 10 wt.% IONP content in the

final composite. The process mirrored the IONP synthesis method, ensuring consistency in material properties.

4.3. Processing method of rutile minerals

For the raw starting material, natural rutile was obtained from Brazil. The access accompanying minerals, particularly Fe_2O_3, were removed by treatment with 0.1 M aqueous oxalic acid solution. The purified rutile was then ground to a particle size below 106 μm using a Retsch planetary ball mill (sample designated as R@000) and further processed *via* nano grinding in a Netzsch MiniCer stirred media mill operating in continuous closed-circuit mode. Samples were collected at various grinding times (30, 60, 150, 180, 240, and 300 minutes), named accordingly (e.g. R@030).

4.4. Equipment utilized for the material property investigations

Scanning and Transmission Electron Microscopy (SEM and TEM)

The particle size, morphology, and microstructure of the prepared nanomaterials and processed minerals were analyzed using a cold field-emission scanning electron microscope, Hitachi S-4700 Type II, which ran at an accelerating voltage of 10 kV to record the micrographs.

Transmission Electron Microscopy (TEM) micrographs were acquired with an FEI Tecnai G2 20 X-TWIN apparatus operating at an accelerating voltage of 200 kV to analyze the nano rutiles' morphology, size, and crystal lattice.

X-ray Powder Diffraction (XRD)

The crystal phase identification and the primary mean crystallite size values were determined by X-ray diffraction analysis, using two different instruments. A Rigaku MiniFlex II diffractometer equipped with a graphite monochromator and functioning with Cu-Kα radiation (λ = 0.15406 nm, 30 kV, 15 mA) and a Shimadzu XRD 6000 diffractometer with a graphite monochromator functioning with CuKα radiation (λ = 1.54 Å, 40 kV, 30 mA) and a Ni filter. The measurement range was sample dependent, and the scanning speed was 1 or 2 (2θ°) min^{-1}. The mean primary crystal size values were determined utilizing the Scherrer equation [10].

Raman Spectroscopy

The sample's crystalline structure was determined using Raman spectroscopy, utilizing two different instruments. A Thermo Scientific DXR confocal Raman microscope equipped with a diode-pumped frequency-doubled Nd:YAG laser. For the acquisition of the Raman spectra, a roughly 1 μm sized spot, 8 mW laser power (8% of its full intensity), a 532 nm laser, and a 10× objective lens were utilized. The resolution of the spectra was 2 cm^{-1}, whereas the pinhole confocal aperture used for each measurement was 25 μm. The second equipment was a Renishaw inVia multilaser confocal Reflex Raman spectrometer equipped with a RenCam CCD detector. The 532 nm laser was utilized as an excitation source, while the spectra were recorded using 100× magnification and the 0.9NA objective. The acquisition time was 30 s, 1800 lines/mm grating for all spectra, and laser power of 20 mW (10% of the maximum laser intensity). The spectral resolution was 4 cm^{-1}.

X-ray Fluorescence (XRF)

The rutile minerals' trace element content was investigated using a Horiba Jobin Yvon XGT-5000 fluorescent spectrometer equipped with a Rh X-ray source. The measurements were carried out at 30 kV excitation voltage, anode current of 0.5 mA, and 1000 s data collection duration.

X-ray photoelectron spectroscopy (XPS)

In FAT mode, XPS spectra of samples were recorded operating a SPECS instrument featuring a PHOIBOS 150 MCD 9 hemispherical electron energy analyzer. The system utilized a monochromatic Al-K source (1486.6 eV), operated at 14 kV and 20 mA. The samples were attached to double-sided adhesive carbon tape and carefully placed to ensure complete coverage by the sample particles. The X-ray source was operated at a power of 200 W, and the pressure in the analysis chamber was maintained between 10^{-9} and 10^{-10} mbar. The binding energy scale was calibrated to the C1s peak at 284.6 eV. High-resolution spectra for all detected elements were acquired with an analyzer pass energy of 20 eV, employing 0.05 eV steps for the analyzed samples. Data analysis was performed utilizing Casa XPS software, with all peaks deconvoluted by applying a Shirley background and Lorentzian–Gaussian line shapes, where the Gaussian–Lorentzian ratio was set to 30.

Diffuse Reflectance Spectroscopy (UV-Vis DRS)

Diffuse Reflectance (DR) spectra of the samples were recorded in the λ=250–800 nm spectral range (with SpectraManager Software) employing a JASCO-V650 diode array computer-controlled spectrophotometer, which was

equipped with an ILV-724 integration sphere. The samples' band gap values were estimated using the Kubelka-Munk function [11].

Specific surface area measurement

The rutile mineral samples' specific surface area was determined by nitrogen adsorption at 77 K, employing a BELCAT-A device. The specific surface area was calculated using the Brunauer, Emmett, and Teller (BET) technique.

Vibrating Sample Magnetometry (VSM)

Magnetic measurements were performed using a vibrating sample magnetometer, 12 T VSM from Cryogenic Limited London, at 300 K, and external magnetic fields up to 5 T. The prepared powders were sealed in epoxy resin for measurements. The saturation magnetizations (M_s) were determined from magnetization isotherms according to the law of approach to saturation (LAS) [12].

4.5. Evaluation of the photocatalytic properties

For the evaluation of the photocatalytic properties, various organic pollutant solutions were prepared with a photocatalyst load of 1 $g \cdot L^{-1}$ (***Table 1***.). For UV-A irradiation, a Pyrex glass reactor was used, with a cooling jacket (25.0 °C), irradiated by six fluorescent lamps (Vilber–Lourmat T-6L UV-A, 6 W power, radiation maximum at 365 nm). The photoreactor used for the visible light experiments was an open glass tube with double walls, equipped with an OSRAM metal halide lamp (Osram Sylvania Inc., Wilmington, MA, USA; Power Star HCl-TC 75W/WDL type) and surrounded by a thermostating jacket

(25.0 °C), containing an aqueous $NaNO_2$ solution (1 M, min. 99.13%) that absorbs UV photons (λ< 400 nm). In both cases, dissolved oxygen concentration was maintained constant by bubbling air through the reactor. Aliquots of 1.5 mL were taken out at specific times, and the concentration changes were followed by a UV-Vis spectrophotometer (Jasco-V650) or a high-performance liquid chromatograph (Hitachi D-7000 HPLC). Prior to the photocatalytic removal tests, stability tests and adsorption tests were conducted in the dark for specific time intervals.

Tabel 1. *Details of the photocatalytic evaluation.*

Tested model pollutants	**Initial concentration of the solution**	**Irradiation type**	**Photocatalyst applied**
(R)-(-)-mellein	10 mM	UV-A	P25
Paracetamol	0.1 mM	UV-A	TH, P25, TH/IONP, P25/IONP
Phenol	0.1 mM	UV-A, Vis	R@ samples
Ibuprofen	0.1 mM	UV-A, Vis	R@030, R@180, R@300

5. Results and discussion

5.1. Investigation of ecotoxicity and photocatalytic removal of a trail pheromone by Evonik AEROXIDE P25 TiO_2.

5.1.1. Investigation of the ecotoxicity of TiO_2 with respect to the foraging behavior of the ant *Lasius niger*.

The ecotoxicity investigations of TiO_2 with respect to ant communication consisted of a negative and a positive control and comparative studies. In the negative control, where both branches of the test bridge were treated with distilled water, ants showed no initial preference, but later favored one side. This preference was explained by the accumulation of pheromone on the respective branch, resulting from the natural behavior of ants during mass recruitment. In contrast, the positive control, where both branches were treated with a TiO_2 suspension, showed no significant preference, supporting the hypothesis that TiO_2 degrades trail pheromones and disrupts the mass recruitment. When given a choice between a water-treated path and one treated with a TiO_2 suspension leading to a food source, ants clearly preferred the water-treated option. Since statistically significant differences emerged only after the third minute of irradiation, the findings point to the degradation of trail pheromones on the TiO_2-treated path under UV-A irradiation, rather than a direct physical disturbance caused by the semiconductor.

5.1.2. Evaluation of the photocatalytic degradation of a pheromone-related organic compound by TiO_2.

To obtain further information on the relationship of TiO_2 and trail pheromones, a photocatalytic degradation experiment was conducted using P25 TiO_2 under UV-A light to remove a trail pheromone component from an aqueous solution. The selected compound, (R)-(-)-3,4-dihydro-8-hydroxy-3-methylisocoumarin ((R)-(-)-mellein), is the trail pheromone of *Formica rufa* ant species and shares structural similarities with the pheromone of *Lasius niger* ((R)-3,4-dihydro-8-hydroxy-3,5,7-trimethylisocoumarin), but is commercially available, unlike the latter. The Evonik Aeroxide P25 TiO_2 removed 62 % of the mellein from the solution during a 120-minute photocatalytic test (***Figure 3.***). The 24-hour room temperature stability test and 120-minute UV-A stability test of mellein, as well as the 60-minute adsorption test with P25, confirmed the reliability of the photocatalytic results.

A photocatalytic degradation process requires two key conditions: aqueous media, provided by rainfall or groundwater in nature, and sufficient UV-A irradiation, which, over the course of a summer day in Europe, can accumulate enough energy to activate TiO_2 and drive photocatalytic reactions [13]. In the light of the above results, it is plausible that the unwanted presence of synthetic TiO_2 in nature can trigger the photocatalytic oxidation of organic compounds in trail pheromones. Given the various significant contributions of ants to their environment, even minor disruptions to their chemical communication have the potential to influence broader environmental processes.

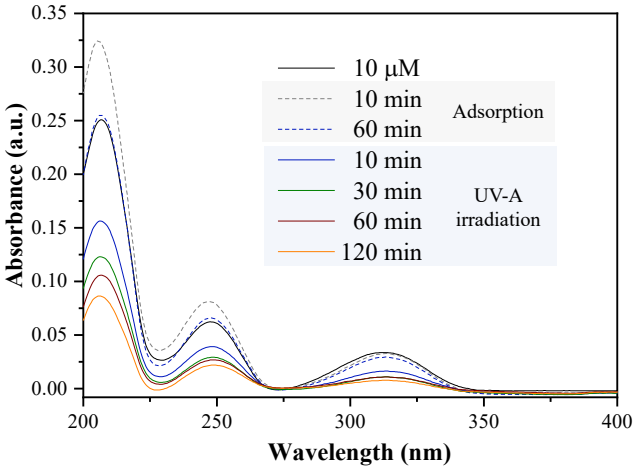

Figure 3. *UV-Vis absorbance spectra showing the adsorption and photocatalytic degradation of mellein.*

5.2. Investigations of Fe_3O_4 loaded TiO_2 photocatalytic systems.

5.2.1. Preparation of magnetically separable Fe_3O_4 loaded TiO_2 composites.

The successful preparation of the P25/IONP and TH/IONP composites was confirmed by the presence of characteristic reflections from both components (i.e., TiO_2 and IONP) in the diffractograms. The pure Fe_3O_4 sample showed strong magnetism without full saturation at 5 T (54.2 emu/g), while composites saturated around 0.8 T with much lower magnetization due to dilution (7.5 and 4.2 emu/g). Even though all the samples exhibit weak ferrimagnetic properties and a superposition of superparamagnetic properties with low coercivity and remanence, they are still suitable for use in magnetic separation.

5.2.2. Assessment of the photocatalytic efficiency of magnetic TiO_2 composites for paracetamol removal under UV light.

Both commercial P25 and synthesized anatase TiO_2 (TH) effectively removed paracetamol, achieving 100% and 95.6% efficiency, respectively (***Figure 4.***). However, when incorporated into composites with IONP, the efficiency of both materials decreased (***Figure 4.***). The partial shielding of active sites of TiO_2 by Fe_3O_4 or the limited photocatalyst content resulting from the 10 wt.% Fe_3O_4 loading has likely contributed to the reduced efficiency.

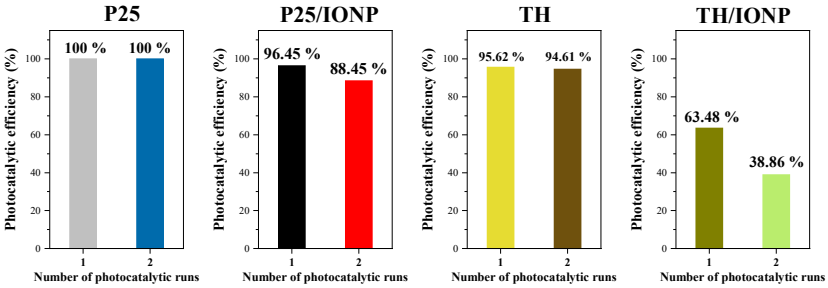

Figure 4. *Photocatalytic efficiency of TiO_2 samples and their magnetic composites for UV light assisted paracetamol removal.*

5.2.3. Evaluation of the separability and reusability of magnetic composites.

Following the first photocatalytic run, the magnetic photocatalysts were collected, dried, and recycled for a second test. During the recycling test, the bare P25 sample showed no change in efficiency, while its composite exhibited a slight decrease in activity (***Figure 4.***). The efficiency of the anatase sample TH remained surprisingly high during the second photocatalytic run (***Figure 4.***). This finding was attributed to degradation intermediates remaining on the

photocatalyst surface after the first cycle, confirmed by chromatograms, which enhanced its hydrophilicity and adsorption properties, thereby indirectly improving its photocatalytic efficiency in the second cycle. The TH/IONP composite exhibited a significant decrease in efficiency, from 63.5% to 38.9%, indicating the need for further structural and compositional investigations to understand the influence of iron oxide on performance.

5.2.4. Investigation of correlations of structural, optical, and surface properties, photocatalytic efficiency, and reusability.

After the photocatalytic and recycling tests, no changes were observed in the crystal structure of the bulk samples. However, the XPS core spectra of Fe2p revealed only Fe^{3+} on the surface of TH/IONP after recycling, indicating oxidation of Fe_3O_4 to Fe_2O_3. In contrast, the magnetite in the P25/IONP composite remained chemically stable. The observed differences in the photocatalytic efficiencies were explained by the different charge transfer mechanisms in the P25-based and the anatase-based composites. In P25/IONP, the band alignment of phases anatase and rutile enables efficient charge separation, protecting magnetite from oxidation, thus maintaining the composite stability. In contrast, the pure anatase TH lacks this synergy, leading to the direct utilization of its photogenerated charges and the gradual oxidation of Fe^{2+} to Fe^{3+}, ultimately producing inactive Fe_2O_3 and hindering hydroxyl radical formation.

5.3. Visible light active natural rutile photocatalyst obtained *via* nano milling [9].

5.3.1. Exploration of a processing method of rutile minerals for use in visible-light-driven photocatalysis.

Following the grinding process, the crystal structure of the obtained seven TiO_2 nano minerals was confirmed to be pure rutile phase (***Figure 5a.***), with decreasing primary crystallite size from 132 nm to 20.1 nm as grinding time increased from 0 to 300 minutes. SEM and TEM (***Figure 5b.***) analyses showed a progressive particle size reduction and increasing homogeneity, with up to 94% of particles reaching ≤0.5 µm in the sample processed for the longest time (***Figure 6.***).

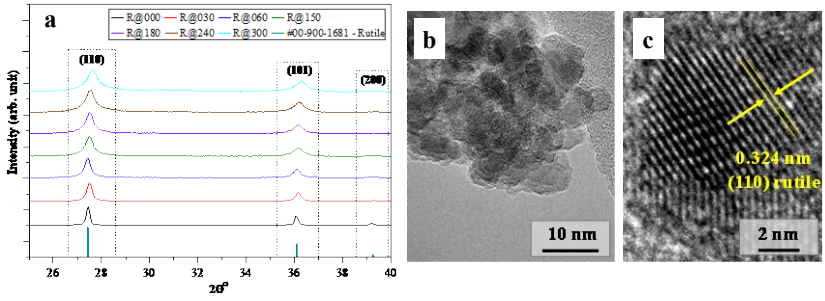

Figure 5. *a. The XRD patterns of the rutile samples obtained after specific grinding times. b. TEM micrographs of the ground natural rutile (R@300). c. The interplanar distance of (110) of rutile observed on TEM micrograph of R@300.*

Despite extensive grinding, the material retained its crystallinity, as confirmed by Raman spectroscopy and the presence of lattice fringes observed in TEM micrographs (***Figure 5c.***). The results highlight the effectiveness of the milling

process in producing nanoscale rutile particles without altering their structural integrity.

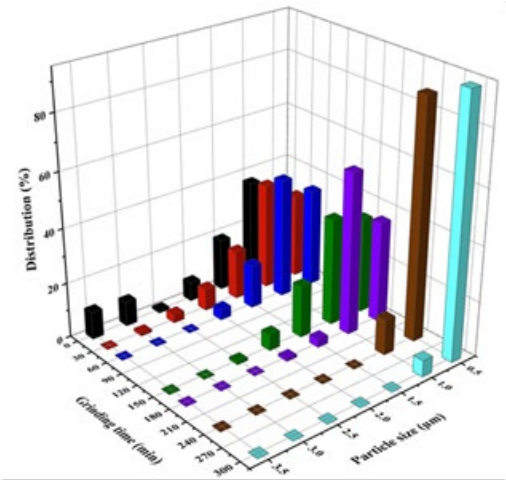

Figure 6. *Particle size distribution histogram of ground natural rutile particles estimated from SEM micrographs.*

5.3.2. Investigation of the structural, optical, and surface properties of the processed minerals.

The ground rutile samples exhibited narrower band gaps (2.4–2.8 eV) than reported in literature for synthetic rutile (3.0 eV), primarily due to the presence of natural dopants like Nb, Nd, Zr, and W, which lead to an extended absorption range in the visible light. As grinding time increased, a gradual widening of the band gap was observed, possibly attributed to two phenomena: the size effect of newly formed nanoparticles (< 10 nm confirmed by TEM) and the slow leaching of dopants during milling. Concurrently, Urbach energy values decreased from 386 to 285 meV, suggesting fewer impurities and improved

structural order despite the mechanical processing. XPS analysis revealed the presence of surface Ti^{3+} species, naturally occurring in rutile in the present case, which are known to enhance photocatalytic activity by promoting •OH radical generation.

5.3.3. Assessment of the photocatalytic performance of natural rutile in removing phenol and ibuprofen under visible light irradiation. & Establishing correlations between material properties and photocatalytic activity.

The results of the photocatalytic tests under visible light show remarkable results: sample R@180 achieved a 33% degradation rate in the case of phenol (***Figure 7.***), with the presence of degradation intermediates confirmed by HPLC measurements.

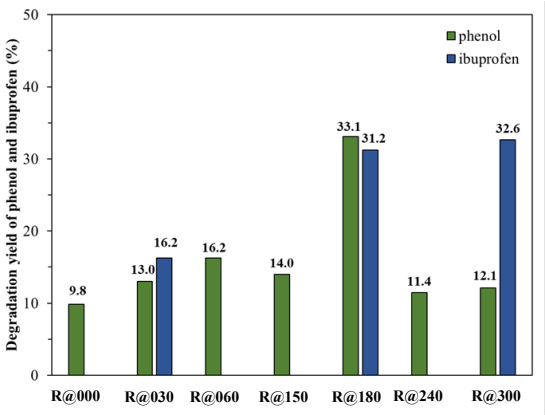

Figure 7. *The photocatalytic performance under visible light irradiation of the nano-milled rutile samples.*

The specific surface area of the samples increased with grinding time, but surface-normalized activity decreased, suggesting a trade-off between surface area and dopant content lost during milling. The higher frequency of 0.5–1 μm particles in samples (e.g, R@180) was linked to enhanced photocatalytic performance in the case of phenol removal. When tested against ibuprofen, all selected samples showed visible light activity, with R@300 achieving the highest degradation rate (32.6%), correlated with the trend of improved activity with reduced particle size.

5.3.4. Analysis of the cost-benefit trade-off between natural rutile mineral and commercial Evonik Aeroxide P25 TiO_2 in heterogeneous photocatalysis applications.

The production of natural rutile photocatalysts *via* wet nano grinding was compared with the synthesis of the commercial Evonik Aeroxide P25, which is known to be manufactured through a flame hydrolysis process. This comparison, conducted on a laboratory scale, considered not only production costs (9.93 €/kg for natural rutile vs. 265 €/kg for synthetic P25) but also environmental impacts, by-products, and photocatalytic efficiency. While synthetic TiO_2 demonstrated strong performance, the natural rutile samples, especially R@180 and R@300, showed promising photocatalytic activity under visible light, with significantly lower production cost normalized to phenol degradation (6.6 €/mmol phenol degraded/h vs. 25 €/mmol phenol degraded/h for P25). The results of the analysis highlight the need for a trade-off between performance and sustainability in the long term.

6. Conclusions

As outlined in the thesis objectives, three aspects of TiO_2 photocatalysts were investigated: their ecotoxicity, their separability and recyclability when incorporated into magnetic composites, and the photocatalytic potential of naturally occurring TiO_2 minerals. Though interdisciplinary, the research is unified by the overarching goal of developing efficient yet environmentally sustainable photocatalytic materials.

In the first part of the thesis, the influence of Evonik Aeroxide P25 TiO_2 on the communication of *Lasius niger* ants was investigated in the frame of foraging tests under laboratory conditions and UV-A irradiation. The tests revealed a statistically significant preference for water-treated pathways over TiO_2-treated ones, and suggested that TiO_2 photocatalytically degraded trail pheromones rather than merely physically disturbing the ants. Additional photocatalytic removal tests of the mellein pheromone component confirmed that TiO_2 can oxidize pheromones, highlighting the material's potential indirect, long-term impacts on the environmental processes.

The second part of the thesis investigated magnetic separation as a promising method for recovering photocatalysts and preventing their release into the environment. Two synthetic TiO_2 photocatalysts – a synthetic anatase sample and the commercial P25 – were introduced in composites with magnetite (Fe_3O_4) and tested for the photocatalytic removal of paracetamol under UV-A irradiation. While P25-Fe_3O_4 composites retained relatively high activity and recyclability, anatase-based composites suffered significant efficiency loss, as well as the partial oxidation of Fe_3O_4 to Fe_2O_3. This deterioration was attributed to the less favorable charge carrier dynamics in the

composite, compared to P25-based samples, where a synergy of anatase and rutile crystal phases is present, facilitating charge separation. The finding underlined the importance of the TiO_2 crystal structure in maintaining composite stability.

In the final research of the thesis, the natural mineral of TiO_2, rutile, was processed through nano-milling and applied for the photocatalytic removal of phenol and ibuprofen. Despite the application of only physical processing methods and no synthetic fine-tuning of the material properties, the nano rutile samples showed remarkable results under visible light irradiation. The photocatalytic properties were correlated with particle size, surface properties, and the presence of naturally occurring dopants (e.g., Nb, Nd, and Zr), which lowered the band gap and enhanced visible-light activation.

A final cost-benefit analysis comparing synthetic Evonik Aeroxide P25 production and nano rutile processing emphasized the trade-off between high photocatalytic performance and long-term environmental feasibility. Both magnetic recovery and naturally sourced rutile mineral photocatalysts can be viable alternatives for sustainability and for the mitigation of the environmental impacts of TiO_2. However, finding the right solution is about striking a balance - every option involves some level of compromise.

7. Scientific Activity

Papers related to the Ph.D. program published up until 25.07.2025

1. **Saszet, K.;** Almási, E.E.; Rácz, Á.; Bohács, K.; Todea, M.; Hernádi, K.; Pap, Z.; Baia, L.

"*Visible Light Active Natural Rutile Photocatalyst Obtained via Nano Milling"*

Molecules, 2025 https://doi.org/10.3390/molecules30071600

I.F.: 4.2 AIS:0.676

Cited: 0 (Google Scholar)

Other papers

2. Tóth, Zs.; Feraru, A.; **Saszet, K.**; Veréb, G.; Vodnar, D. C.; Todea, M.; Timar-Gabor, A.; Dave, A. K.; Sand, D.; Dreanca, A.; Magyari, K.; Baia, L.

"Relation between shape-tailored CeO_2 nanoparticles morphology and hemocompatibility and antimicrobial effect"

Biomaterials Advances, 2025 https://doi.org/10.1016/j.bioadv.2025.214229

I.F.: 5.5

Cited: 0 (Google Scholar)

3. Bobu, E.; **Saszet, K.**; Tóth, Z.-R.; Páll, E.; Gyulavári, T.; Baia, L.; Magyari, K.; Baia, M.

"*TiO_2–Alginate–Chitosan-Based Composites for Skin Tissue Engineering Applications"*

Gels, 2024 https://doi.org/10.3390/gels10060358

I.F.: 5.0

Cited: 5 (Google Scholar)

4. Nikita Sharma, N.; **Saszet, K.**; Szabó, T.; Karajz, D.; Szilágyi, I. M.; Garg, S.; Pap, Zs.; Hernádi, K.

"Demonstration of effectiveness: Plant extracts in the tuning of BiOX photocatalysts' activity"

Catalysis Today, 2023 https://doi.org/10.1016/j.cattod.2022.12.015

I.F.: 5.2

Cited: 7 (Google Scholar)

5. Cadiș, A. I.; Mureșan, L. E.; Perhaița, I.; Pop, L. C.; **Saszet, K.**; Barbu-Tudoran, L.; Borodi, G;

"Peculiarities on methyl orange adsorption by porous $ZnIn_2S_4$ prepared in different conditions"

Journal of Nanoparticle Research, 2022 https://doi.org/10.1007/s11051-022-05458-8

I.F.: 2.5

Cited: 5 (Google Scholar)

6. Stingescu, L.; Cadar, C.; Cotet, L.C.; Baia, L.; **Saszet, K.**; Magyari, K.; Mihis, A. G.; Fort, C.I.; Stroe, M.; Matei, E.; Nila, A.; Anghel, I.; Baia, M.; Baibarac, M.; Danciu, V.;

"Morphological and structural investigation of the poly (vinyl chloride) / graphene oxide composites"

Studia UBB Chemia, 2020 https://doi.org/10.24193/subbchem.2020.3.19

I.F.: 0.447

Cited: 3 (Google Scholar)

Publications before Ph.D. studies

7. Kása, Zs.; **Saszet, K.**, Dombi, A.; Hernádi, K.; Baia, L.; Magyari, K.; Pap, Zs.

"Thiourea and Triton X-100 as shape manipulating tools or more for Bi_2WO_6 photocatalysts?"

Materials Science in Semiconductor Processing, 2018

https://doi.org/10.1016/j.mssp.2017.10.001

I.F.: 2.722

Cited: 13 (Google Scholar)

8. Vajda, K; **Saszet, K.**; Kedves, Zs.; Kása, Zs.; Danciu, V.; Baia, L.; Magyari, K.; Hernádi, K.; Kovács, G.; Pap, Zs.

"Shape-controlled agglomeration of TiO_2 nanoparticles. New insights on polycrystallinity vs. single crystals in photocatalysis"

Ceramics International, 2016

https://doi.org/10.1016/j.ceramint.2015.10.095

I.F.: 2.986

Cited: 38 (Google Scholar)

9. Baia, L.; Orbán, E.; Fodor, Sz.; Hampel, B.; Kedves, E. Zs.; **Saszet, K.**; Székely, I.; Karácsonyi, É.; Réti, B., Berki, P.; Vulpoi, A.; Magyari, K.; Csavdári, A.; Bolla, Cs; Coșoveanu, V.; Hernádi, K.; Baia, M.; Dombi, A.; Danciu, V.; Kovács,G.; Pap, Zs.

"Preparation of TiO_2/WO_3 composite photocatalysts by the adjustment of the semiconductors' surface charge"

Materials Science in Semiconductor Processing, 2016

https://doi.org/10.1016/j.mssp.2015.08.042

I.F.: 2.359

Cited: 48 (Google Scholar)

Non-ISI listed publications

1. Almási, E.; Pap, Zs.; **Saszet, K.**; Gyulavári, T.; Rácz, Á.; Mucsi, G.; Halyag, N.; Rákhely, G. *"Fine structural features of ilmenite achieved by wet milling and its potential in the degradation of pollutants in wastewater"*, Geosciences and Engineering (HU ISSN 2063-6997), Vol. 8, No. 12 (2020), pp. 251–263.
2. Almási, E.; Pap, Zs.; **Saszet, K.**; Rácz, Á.; Mucsi, G.; Halyag, N.; Rákhely, G. "*Structure stability and properties of nano milled cuprite and its applicability in wastewater treatment"*, Geosciences and Engineering (HU ISSN 2063-6997), Vol. 8, No. 12 (2020), pp. 238–250.

Conference participations

Ph.D. related conferences

1. **Kata Saszet**, Zsolt Pap, Lucian Baia, Klára Hernádi "*Comparison of different $FeTiO_3$ containing systems based on their structural and possible photocatalytic properties*", 6th European Conference on Environmental Applications of Advanced Oxidation Processes (EAAOP-6), 26-30 June 2019, Portoroz, Slovenia - *poster presentation*

2. **Kata Saszet**, Eszter Mátyás, Zsolt Czekes, Enikő- Eszter Almási, Zsolt Pap "*Comparative study on the toxic effect of synthetic nano-ilmenite and natural ilmenite mineral on Formica pratensis*", 8th Central European Workshop of Myrmecology, 27-30 September 2019, Regensburg, Germany - *poster presentation*

3. **Kata Saszet**, Zsolt Pap, Zsolt Czekes, Enikő-Eszter Almási, Lucian Baia "*Structural and Toxicity Studies of Synthetic and Mineral Origin Iron (II) Titanate*", 25th International Conference on Chemistry, 24–26 October 2019, Cluj-Napoca, Romania - *oral presentation*

4. **Kata Saszet**, Enikő-Eszter Almási, Zsolt Pap, Lucian Baia "*Cuprite minerals – investigation of material properties and possible applications in chemistry*", XXVIth International Conference on Chemistry, 30 October 2020, virtual conference – *oral presentation*

5. Simona Halmagyi, Lucian Pop, **Kata Saszet** *"Synthesis, optimization and characterization of iron oxide nanoparticles obtained by co-precipitation method"*, 9th European Young Engineers Conference, 19-21 April 2021, virtual conference – *oral presentation*

6. **Kata Saszet**, Zsolt Czekes, Lucian Baia, Enikő-Eszter Almási, Ádám Rácz, Gábor Rákhely, Klára Hernádi and Zsolt Pap *"Natural Photocatalyst: Real Alternatives to the Synthesized Ones?"*, The 5th International Conference on New Photocatalytic Materials for Environment, Energy and Sustainability (NPM-5), 24-27 May 2021, virtual conference - *oral presentation*

7. **Kata Saszet**, Enikő-Eszter Almási, Zsolt Pap, Klára Hernádi, Lucian Baia "Cuprite minerals: material properties, changes due to processing and possible application in photocatalysis", European Materials Research Society

(E-MRS) 2021 Spring Meeting, May 31 - June 3 2021, virtual conference – *poster presentation*

8. **Kata Saszet**, Darius Groza, Simona Halmagyi, Enikő-Eszter Almási, Zsolt Pap, Lucian Baia "*The influence of the source of magnetic particles on the photocatalytic properties of TiO_2/MP composites*", European Materials Research Society (E-MRS) 2021 Fall Meeting, 20-23 September 2021, virtual conference – *poster presentation*

9. Kata Saszet, Simona Halmagyi, Eszter Mátyás, Lucian Pop, Zsolt Czekes, Zsolt Pap, Lucian Baia "*TiO_2 P25/Fe_3O_4/ γ-Fe_2O_3 photocatalytically active nanocomposites and the ecotoxicological effects of TiO_2 P25 on the Lasius niger ant species*", 12th International Conference on Physics of Advanced Materials (ICPAM-13), 24-30 September 2021, Sant Feliu de Guixols, Spain - *oral presentation and* ***Augustin Mayor Prize for the best oral presentation delivered by a young scientist.***

10. **Kata Saszet**, Simona Halmagyi, Darius Groza, Enikő-Eszter Almási, Zsolt Pap, Lucian Baia "*Natural and synthetic components in TiO_2/magnetic NP composites and their photocatalytic applicability",* 5th EuChemS Conference on Green and Sustainable Chemistry (5th EuGSC), 26-29 September 2021, virtual conference - *poster presentation*

11. **Kata Saszet**, Nikita Sharma, Zsolt Czekes, Zsolt Pap, Lucian Baia "*Photocatalytic Effect of Evonik Aeroxide P25 TiO_2 on the Trail Pheromones of Different Ant Species*", 11th European Conference on Solar Chemistry and Photocatalysis: Environmental Applications (SPEA11), 6-10 June 2022, Turin, Italy - *poster presentation*

Other conferences

12. Nikita Sharma, **Kata Saszet,** Zsolt Pap, Klára Hernádi "*Use Of Plant Extracts to Enhance the Photocatalytic Response of Bismuth Oxyhalides*", 11th European Conference on Solar Chemistry and Photocatalysis: Environmental Applications (SPEA11), 6-10 June 2022, Turin, Italy – *poster presentation*

13. Zsejke-Réka Tóth, Gabor Alida Timar, Alexandra Feraru, **Kata Saszet**, Dan C. Vondar, Milica Todea, Aditi Dave K., Alexandra Dreanca, Emilia Licarete, Gábor Veréb, Lucian Baia, Klára Magyari "*Effect of different shaped cerium oxide nanoparticles on wound healing",* 30th International Conference on Chemistry, 23-26 October 2024, Cluj-Napoca, Romania – *oral presentation*

8. References

[1] X. Li, X. Shen, W. Jiang, Y. Xi, S. Li, Comprehensive review of emerging contaminants: Detection technologies, environmental impact, and management strategies, Ecotoxicol Environ Saf 278 (2024) 116420. https://doi.org/10.1016/j.ecoenv.2024.116420.

[2] B. Ohtani, Photocatalysis by inorganic solid materials, in: 2011: pp. 395–430. https://doi.org/10.1016/B978-0-12-385904-4.00001-9.

[3] A. Fujishima, K. Honda, Electrochemical Photolysis of Water at a Semiconductor Electrode, Nature 238 (1972) 37–38. https://doi.org/10.1038/238037a0.

[4] J.A. Rengifo-Herrera, C. Pulgarin, Why five decades of massive research on heterogeneous photocatalysis, especially on TiO_2, has not yet driven to water disinfection and detoxification applications? Critical review of drawbacks and challenges, Chemical Engineering Journal 477 (2023) 146875. https://doi.org/10.1016/j.cej.2023.146875.

[5] T.Y. Sun, N.A. Bornhöft, K. Hungerbühler, B. Nowack, Dynamic Probabilistic Modeling of Environmental Emissions of Engineered Nanomaterials, Environ Sci Technol 50 (2016) 4701–4711. https://doi.org/10.1021/acs.est.5b05828.

[6] T. Ayorinde, C.M. Sayes, An updated review of industrially relevant titanium dioxide and its environmental health effects, Journal of Hazardous Materials Letters 4 (2023) 100085. https://doi.org/10.1016/j.hazl.2023.100085.

[7] J. López, A. Rey, E. Viñuelas-Zahinos, P.M. Álvarez, Preparation of a new green magnetic Fe_3O_4 @TiO_2-P25 photocatalyst for solar advanced oxidation processes in water, J Environ Chem Eng 11 (2023) 109999. https://doi.org/10.1016/j.jece.2023.109999.

[8] F. Heidarinejad, H. Kamani, A. Khtibi, Magnetic Fe-doped TiO_2@Fe_3O_4 for metronidazole degradation in aqueous solutions: Characteristics and efficacy assessment, Heliyon 9 (2023) e21414. https://doi.org/10.1016/j.heliyon.2023.e21414.

[9] K. Saszet, E.E. Almási, Á. Rácz, K. Bohács, M. Todea, K. Hernádi, Z. Pap, L. Baia, Visible Light Active Natural Rutile Photocatalyst Obtained via Nano Milling, Molecules 30 (2025) 1600. https://doi.org/10.3390/molecules30071600.

[10] Md. Sahadat Hossain, S. Ahmed, Easy and green synthesis of TiO_2 (Anatase and Rutile): Estimation of crystallite size using Scherrer equation, Williamson-Hall plot, Monshi-Scherrer Model, size-strain plot,

Halder- Wagner Model, Results in Materials 20 (2023) 100492. https://doi.org/10.1016/j.rinma.2023.100492.
[11] S. Landi, I.R. Segundo, E. Freitas, M. Vasilevskiy, J. Carneiro, C.J. Tavares, Use and misuse of the Kubelka-Munk function to obtain the band gap energy from diffuse reflectance measurements, Solid State Commun 341 (2022) 114573. https://doi.org/10.1016/j.ssc.2021.114573.
[12] H. Zhang, D. Zeng, Z. Liu, The law of approach to saturation in ferromagnets originating from the magnetocrystalline anisotropy, J Magn Magn Mater 322 (2010) 2375–2380. https://doi.org/10.1016/j.jmmm.2010.02.040.
[13] N. Proutsos, S. Alexandris, A. Liakatas, P. Nastos, I.X. Tsiros, PAR and UVA composition of global solar radiation at a high altitude Mediterranean forest site, Atmos Res 269 (2022) 106039. https://doi.org/10.1016/j.atmosres.2022.106039.